frontiers in Materials

ORIGINAL RESEARCH
published: 30 November 2021
doi: 10.3389/fmats.2021.774612

Hybrid Bandgaps in Mass-coupled Bragg Atomic Chains: Generation and Switching

Shao-Feng Xu[1], *Zhu-Long Xu*[1] *and Kuo-Chih Chuang*[1,2]*

[1]*Key Laboratory of Soft Machines and Smart Devices of Zhejiang Province, School of Aeronautics and Astronautics, Institute of Applied Mechanics, Zhejiang University, Hangzhou, China,* [2]*State Key Laboratory for Strength and Vibration of Mechanical Structures, School of Aerospace Engineering, Xi'an Jiaotong University, Xi'an, China*

In this work, without introducing mass-in-mass units or inertial amplification mechanisms, we show that two Bragg atomic chains can form an acoustic metamaterial that possesses different types of bandgaps other than Bragg ones, including local resonance and inertial amplification-like bandgaps. Specifically, by coupling masses of one monatomic chain to the same masses of a diatomic or triatomic chain, hybrid bandgaps can be generated and further be switched through the adjustment of the structural parameters. To provide a tuning guidance for the hybrid bandgaps, we derived an analytical transition parameter (p-value) for the mass-coupled monatomic/diatomic chain and analytical discriminants for the mass-coupled monatomic/triatomic chain. In our proposed mass-coupled monatomic/triatomic chain system, each set of analytical discriminants determines a hybrid bandgap state and a detailed examination reveals 14 different bandgap states. In addition to bandgap switching, the analytical p-value and discriminants can also be used as a guide for designing the coupled-chain acoustic metamaterials. The relations between the mass-coupled monatomic/triatomic chain system and a three-degree-of-freedom (DOF) inertial amplification system further indicate that the band structure of the former is equivalent to that of the latter through coupling masses by negative dynamic stiffness springs.

Keywords: metamaterials, atomic chains, bandgaps, local resonance, inertial amplification, phononic crystal

OPEN ACCESS

Edited by:
Yan-Feng Wang,
Tianjin University, China

Reviewed by:
Yabin Jin,
Tongji University, China
Yongquan Liu,
Xi'an Jiaotong University, China

***Correspondence:**
Kuo-Chih Chuang
chuangkc@zju.edu.cn

Specialty section:
This article was submitted to Metamaterials, a section of the journal Frontiers in Materials

Received: *12 September 2021*
Accepted: *27 September 2021*
Published: *30 November 2021*

Citation:
Xu S-F, Xu Z-L and Chuang K-C (2021) Hybrid Bandgaps in Mass-coupled Bragg Atomic Chains: Generation and Switching. Front. Mater. 8:774612. doi: 10.3389/fmats.2021.774612

INTRODUCTION

Being classic textbook models that can explain lattice vibrations in solid state physics, one-dimensional atomic chains can capture the most fundamental properties of phononic crystals (PCs) (Kittel et al., 1996; Hofmann, 2015), which are known for having Bragg bandgaps that can suppress the propagation of mechanical waves (Deymier, 2013; Khelif and Adibi, 2015). Over the past decade, based on PCs that contain the simplest spring-mass systems in a unit cell, some important advances in the domains of nonlinear wave guides (Narisetti et al., 2010; Porubov and Andrianov, 2013; Ganesh and Gonella, 2015; Fang et al., 2016), topological edge states (Pal et al., 2018; Al Ba'ba'a et al., 2019), and diode-like acoustic structures (Vila et al., 2017; Attarzadeh et al., 2018) have been achieved. The atomic chains have also been used to explain nonlocal interactions of the panels of origami metamaterials (Pratapa et al., 2018). Despite being an idealized spring-mass lattice system, the simplest atomic chains can capture the bandgap phenomenon of PCs and to which other bandgap-generation mechanisms can be introduced.

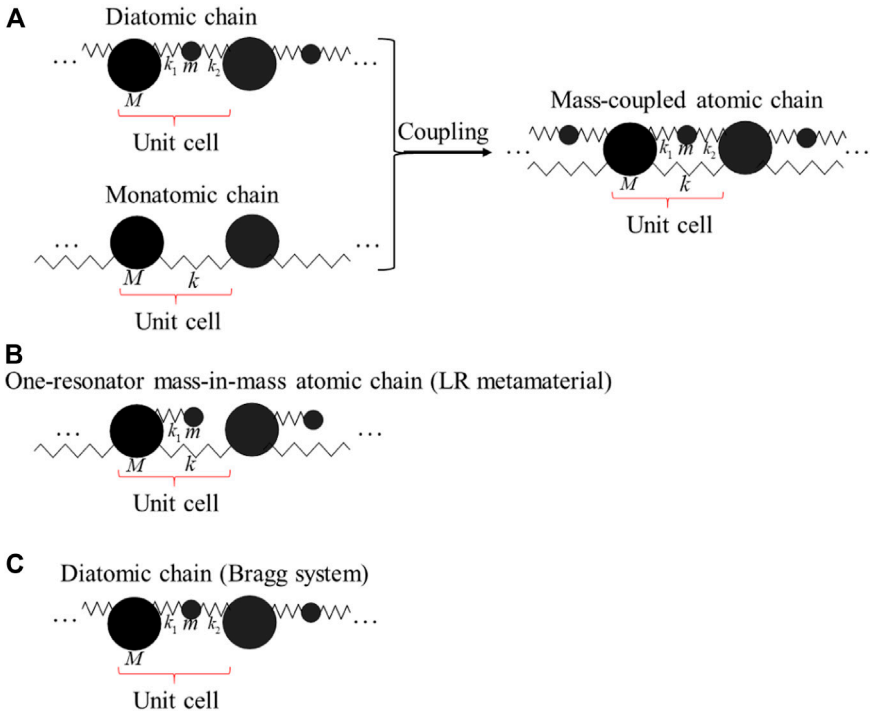

FIGURE 1 | (A) The mass-coupled atomic chain coupled by a diatomic chain and a monatomic chain. **(B)** One-resonator mass-in-mass atomic chain. **(C)** Diatomic chain.

Since the properties of the Bragg bandgaps depend heavily on the lattice constant, it is difficult to achieve low-frequency bandgaps if not increasing the size of the periodic cell. By introducing mass-in-mass units to a monatomic lattice system, acoustic metamaterials exhibiting local resonance (LR) bandgaps independent of the spatial periodicity can be obtained (Huang et al., 2009). Acoustic metamaterials have attracted significant interest due to their unusual mechanical properties such as subwavelength bandgaps, negative effective mass density, or negative effective modulus (Liu et al., 2000; Li and Chan, 2004; Fang et al., 2006; Lazarov and Jensen, 2007; Yao et al., 2008; Huang and Sun, 2010; Huang and Sun, 2012). The concept of infinite mass-in-mass atomic chains have been extended to the design of continuum structures such as elastic metamaterial rods (i.e., through the homogenization method), beams, plates or pillared metamaterial (i.e., surfaces that consist of pillars or branching substructures) in which longitudinal, lateral or flexural vibrations can be suppressed (Yu et al., 2006; Kundu et al., 2014; Zhu et al., 2014; Liu et al., 2015; MuhammadLim, 2019; Jin et al., 2021). Although LR bandgaps are low-frequency ones compared to Bragg bandgaps, several researchers have attempted to further push the bandgaps to lower frequencies without adding extra masses. By introducing internal couplings to mass-in-mass lattices through negative stiffness springs, Hu *et al.* recently showed that multiple bandgaps and ultra-low resonance bandgaps can be achieved without adding extra masses (Hu et al., 2017; Hu et al., 2019). In addition to mass-in-mass units, inertial amplification mechanisms have also been introduced to mass-spring chains to generate wide and deep low-frequency bandgaps (Yilmaz et al., 2007; Yilmaz and Hulbert, 2010; Taniker and Yilmaz, 2013; Yilmaz et al., 2017). Frandsen *et al.* investigated an elastic rod with a periodically attached inertial amplification mechanism and found the characteristic double-peak phenomenon in bandgap regions (Frandsen et al., 2016). Through deriving the effective mass of a modified monatomic chain with a lightweight attached mass-link system, Bennetts *et al.* obtained its low-frequency vibration-isolation properties (Bennetts et al., 2019). Recently, Li and Zhou proposed a periodic mass-spring-truss chain based on a scissor-like structure and inertial amplification to achieve low-frequency vibration attenuation (Li and Zhou, 2021). One interesting question arises: Can we generate local resonance or inertial amplification bandgaps in the band structures of atomic chains without mass-in-mass units or inertial amplification mechanisms?

To solve the above question, we introduce mass coupling to two Bragg atomic chains at certain masses. Specifically, as illustrated in **Figure 1A**, considering a fundamental configuration of a mass-coupled atomic chain, where a diatomic chain is coupled to a monatomic chain. It is well known that, depending on the existence of certain springs, the mass-coupled atomic chain can be degenerated to a local resonant (LR) acoustic metamaterial with mass-in-mass units (*see* **Figure 1B**) or an alternating mass-spring Bragg system (i.e., also known as phononic crystal) showed in **Figure 1C**. What we are going to demonstrate is that the local resonance, as

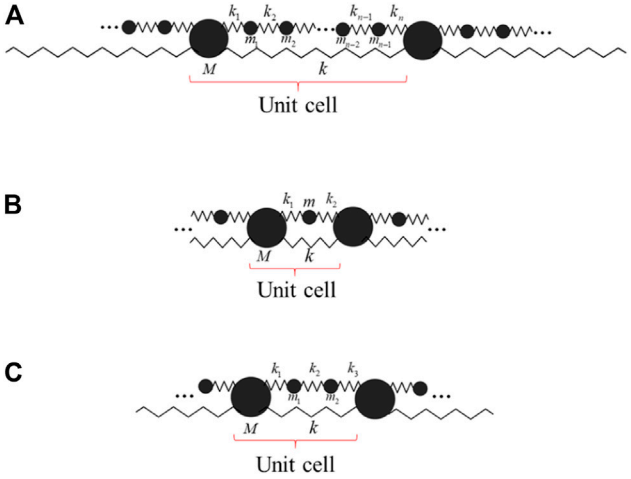

FIGURE 2 | (A) The mass-coupled atomic chain with $n-1$ different masses between coupled masses in a unit cell (n-DOF), **(B)** The mass-coupled monatomic/diatomic chain (2-DOF), **(C)** The mass-coupled monatomic/triatomic chain (3-DOF).

well as the inertial amplification-like (IA-like) bandgaps can be opened through adjusting parameters without altering system configuration (i.e., without performing mechanical cutting of certain springs or arranging the inertial amplification mechanisms).

In this work, we first obtain the governing equations of the mass-coupled atomic chain with n-degree-of-freedom (DOF) by analytical mechanics. Then, the analytical expressions of band structures, anti-resonant frequencies, and edge frequencies of passbands are deduced. In **Section 3.1**, through discussions about mass-coupled monatomic/diatomic chain, we show that LR bandgaps can be generated simply by performing parametric switching, which is characterized by an inherent transition parameter (p-value). The different bandgap behaviors of mass-coupled monatomic/triatomic chain are classified by different sets of discriminants in **Section 3.2**. Finally, the relations between the mass-coupled monatomic/triatomic chain system and a 3-DOF inertial amplification system are further discussed in **Section 3.3**.

MODEL DESCRIPTIONS AND TRANSITION CONDITIONS OF HYBRID BANDGAPS

The mass-coupled atomic chain, as illustrated in **Figure 1A**, can be generalized as a model shown in **Figure 2A**, where a polyatomic chain is coupled to a monatomic chain. There are arbitrary $n-1$ $(n\geq 2)$ masses connected by n different springs between coupled masses in a unit cell. Obviously, there are n degrees of freedom in this system, the displacements of the coupled mass M_j and other masses $m_{i,j}(1\leq i\leq n-1)$ are respectively marked as $U_j$and $u_{i,j}$ for the j-th unit cell.

The band structures of this infinite mass-coupled atomic chain can be deduced as follows. First, we list all expressions about kinetic and potential energies related to the displacements:

$$\begin{cases} T=\dfrac{1}{2}m_{1,j}\dot{u}_{i,j}^2 \\ V=\dfrac{1}{2}k_1\left(u_{1,j}-U_j\right)^2+\dfrac{1}{2}k_2\left(u_{1,j}-u_{2,j}\right)^2,\ \text{for } i=1, \end{cases} \tag{1}$$

$$\begin{cases} T=\dfrac{1}{2}m_{i,j}\dot{u}_{i,j}^2 \\ V=\dfrac{1}{2}k_i\left(u_{i,j}-u_{i-1,j}\right)^2+\dfrac{1}{2}k_{i+1}\left(u_{i,j}-u_{i+1,j}\right)^2,\ \text{for } 2\leq i\leq n-2, \end{cases} \tag{2}$$

$$\begin{cases} T=\dfrac{1}{2}m_{n-1,j}\dot{u}_{n-1,j}^2 \\ V=\dfrac{1}{2}k_n\left(u_{n-1,j}-U_{j+1}\right)^2+\dfrac{1}{2}k_{n-1}\left(u_{n-1,j}-u_{n-2,j}\right)^2,\ \text{for } i=n-1, \end{cases} \tag{3}$$

And

$$\begin{cases} T=\dfrac{1}{2}M_j\dot{U}_j^2 \\ V=\dfrac{1}{2}k_1\left(U_j-u_{1,j}\right)^2+\dfrac{1}{2}k_n\left(U_j-u_{n-1,j-1}\right)^2+\dfrac{1}{2}k\left(U_j-U_{j-1}\right)^2+\dfrac{1}{2}k\left(U_j-U_{j+1}\right)^2. \end{cases} \tag{4}$$

According to the Lagrange equation for conservative systems, i.e.,

$$\frac{\partial L}{\partial \bar{u}}-\frac{d}{dt}\left(\frac{\partial L}{\partial \dot{\bar{u}}}\right)=0, \tag{5}$$

Where $L=T-V$ is Lagrangian, $\bar{u}$ is generalized displacement, and $\dot{\bar{u}}$ is generalized velocity, the governing equations can be derived as

$$\begin{cases} m_{1,j}\ddot{u}_{1,j}+k_1\left(u_{1,j}-U_j\right)+k_2\left(u_{1,j}-u_{2,j}\right)=0 \\ m_{i,j}\ddot{u}_{i,j}+k_i\left(u_{i,j}-u_{i-1,j}\right)+k_{i+1}\left(u_{i,j}-u_{i+1,j}\right)=0 \quad (2\leq i\leq n-2) \\ m_{n-1,j}\ddot{u}_{n-1,j}+k_n\left(u_{n-1,j}-U_{j+1}\right)+k_{n-1}\left(u_{n-1,j}-u_{n-2,j}\right)=0 \\ M_j\ddot{U}_j+k_1\left(U_j-u_{1,j}\right)+k_n\left(U_j-u_{n-1,j-1}\right)+k\left(2U_j-U_{j-1}-U_{j+1}\right)=0. \end{cases} \tag{6}$$

Then the band structures can be obtained by solving the following eigenvalue problem according to Bloch theorem (Huang et al., 2009; Hu et al., 2017; Hu et al., 2019):

$$\left|\mathbf{K}-\boldsymbol{\omega}^2\mathbf{M}\right|=\mathbf{0}, \tag{7}$$

Where

$$\mathbf{K}=\begin{bmatrix} 2k\left(1-\cos(qa)\right)+k_1+k_n & -k_1 & 0 & \cdots & 0 & -k_ne^{-iqa} \\ -k_1 & k_1+k_2 & -k_2 & \cdots & \cdots & 0 \\ 0 & -k_2 & \ddots & \ddots & \cdots & \vdots \\ \vdots & \cdots & \ddots & \ddots & -k_{n-2} & 0 \\ 0 & \cdots & \cdots & -k_{n-2} & k_{n-2}+k_{n-1} & -k_{n-1} \\ -k_ne^{iqa} & 0 & \cdots & 0 & -k_{n-1} & k_{n-1}+k_n \end{bmatrix}, \tag{8}$$

$$\mathbf{M}=\begin{bmatrix} M_j & 0 & 0 & \cdots & 0 & 0 \\ 0 & m_{1,j} & 0 & \cdots & \cdots & 0 \\ 0 & 0 & \ddots & \ddots & \cdots & \vdots \\ \vdots & \cdots & \ddots & \ddots & 0 & 0 \\ 0 & \cdots & \cdots & 0 & m_{n-2,j} & 0 \\ 0 & 0 & \cdots & 0 & 0 & m_{n-1,j} \end{bmatrix},$$

q is the Bloch wave vector, ω is circular frequency, and a is lattice constant.

The coefficient polynomial of **Eq. 7** can be expressed as

$$2x\left[\prod_{i=1}^{n}k_i+k\left(\prod_{i=1}^{n-1}m_i\right)f_1(\omega)\right]-\omega^2\left(\prod_{i=1}^{n}m_i\right)f_2(\omega)=0, \tag{9}$$

Where

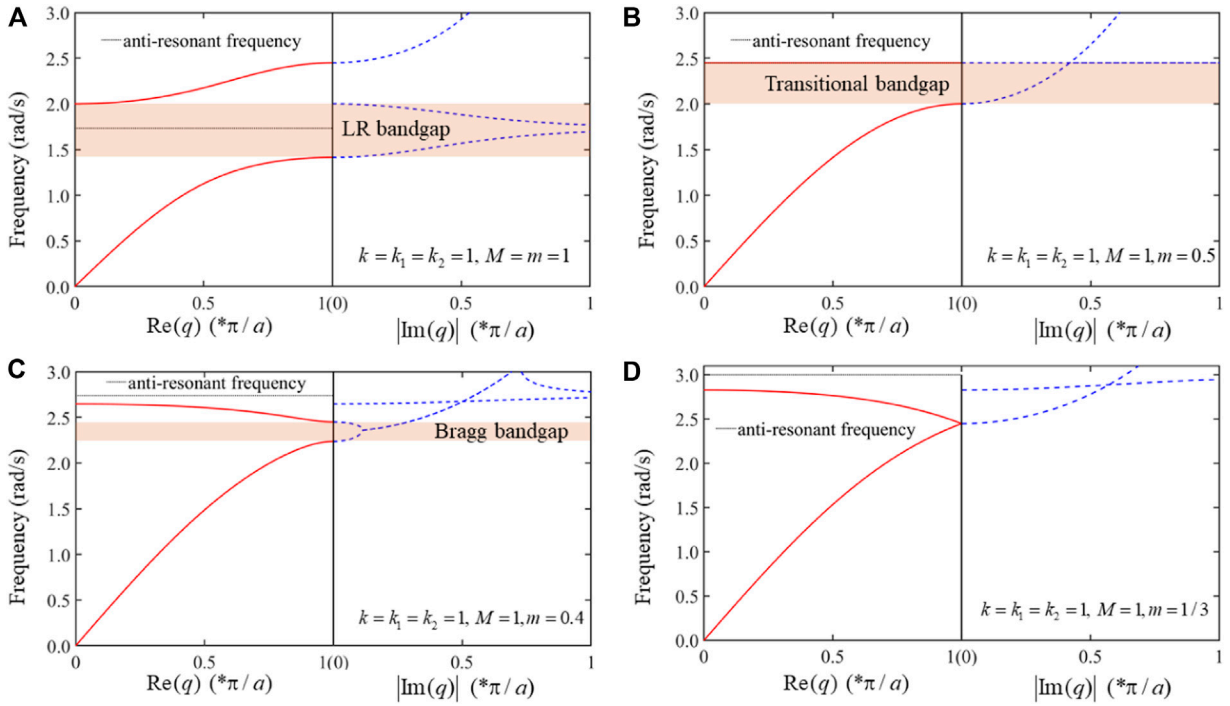

FIGURE 3 | Band structures of the mass-coupled monatomic/diatomic chain (2-DOF). **(A)** The anti-resonant frequency is between the adjacent frequencies at$q = 0\,(x = 0)$ corresponding to$p > 1$, **(B)** the anti-resonant frequency line coincides with a passband curve corresponding to$p = 1$, **(C)** the anti-resonant frequency is outside two adjacent frequencies corresponding to$p < 1$, **(D)** $p < 1$ and Bragg bandgap disappears.

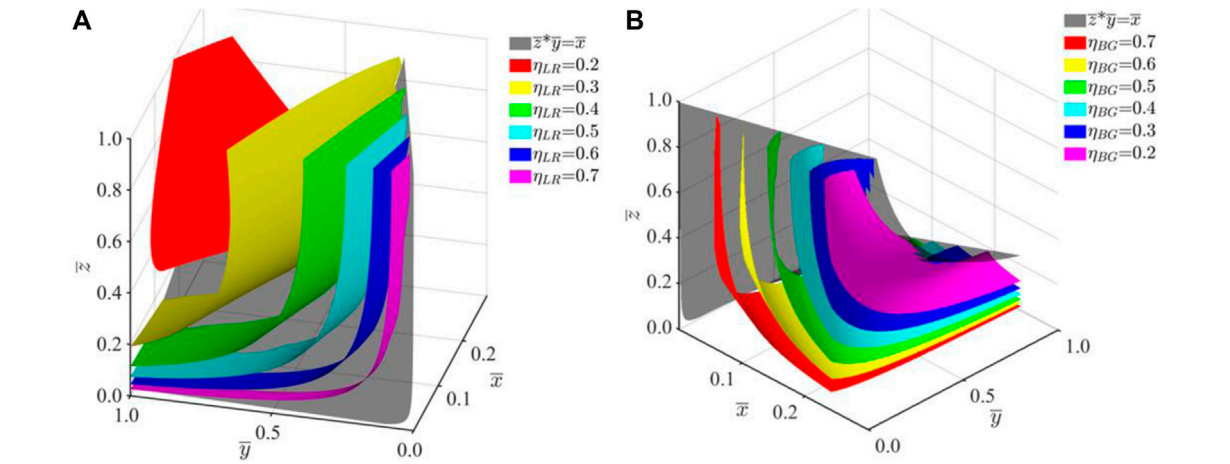

FIGURE 4 | Isosurfaces of the ratios of the width of bandgap region to the maximum frequency of passbands for **(A)** LR bandgap, and **(B)** Bragg bandgap.

$$\begin{cases} x = 1 - \cos(qa) \\ m_i = m_{i,j}\,(1 \le i \le n-1), \\ m_n = M = M_j \end{cases} \tag{10}$$

And the analytical formulas of $f_1(\omega)$ and $f_2(\omega)$ are listed in **Appendix A**. Coefficient polynomial of x determines the existence of the anti-resonant frequencies as well as their values according to **Eq. 9** (Hu et al., 2017; Yilmaz et al., 2017; Bennetts et al., 2019; Hu et al., 2019; Li and Zhou, 2021). So anti-resonant frequencies are acquired by solving the following expression:

$$\prod_{i=1}^{n} k_i + k\left(\prod_{i=1}^{n-1} m_i\right) f_1(\omega) = 0. \tag{11}$$

It is worth noting that in band structures any single curve of passbands is continuous when $q \in (0, \frac{\pi}{a})\,(x \in (0, 2))$. Meanwhile,

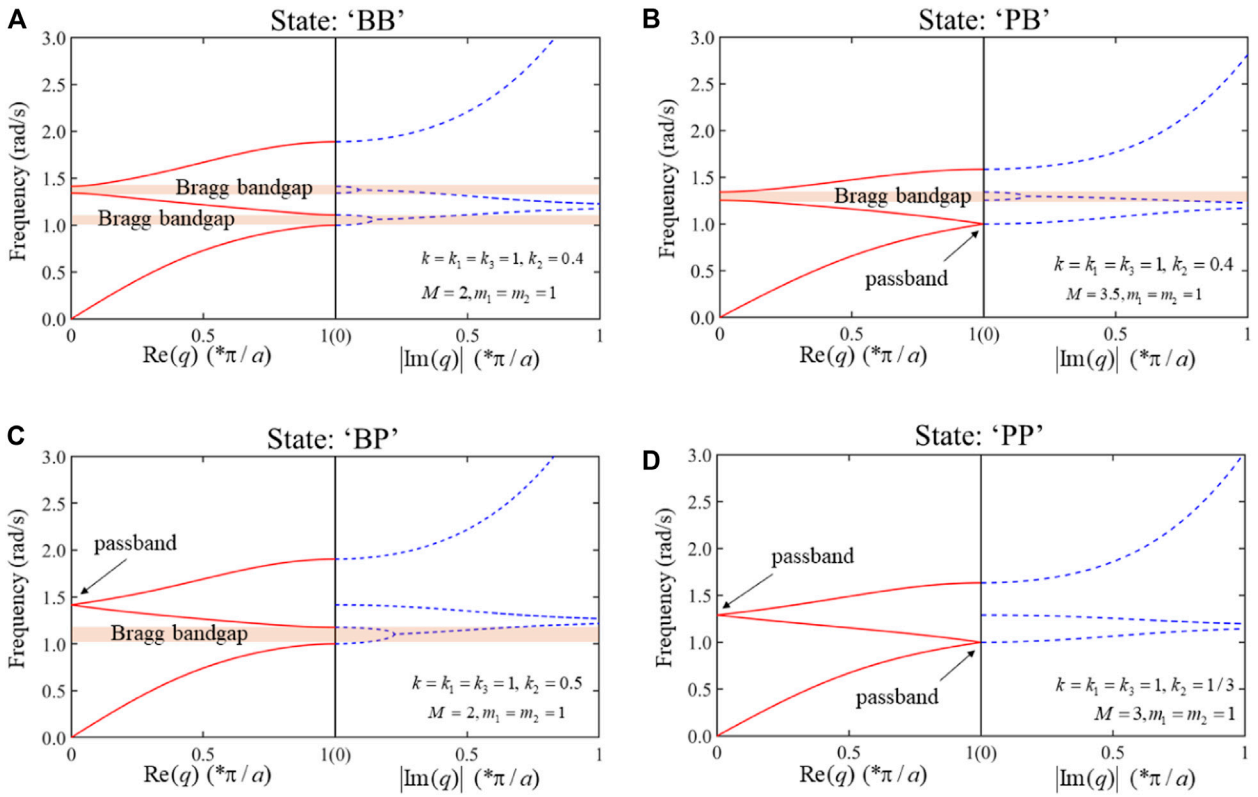

FIGURE 5 | Different bandgap states when anti-resonant frequencies are absent in the mass-coupled monatomic/triatomic chain system. **(A)** State "BB": the first and second bandgaps are Bragg bandgaps. **(B)** State "PB": the first Bragg bandgap closes. **(C)** State "BP": the second Bragg bandgap closes. **(D)** State "PP": both first and second bandgaps disappear.

the passbands will not intersect with the anti-resonant frequency line. According to **Eq. 9**, if an anti-resonant frequency solved by **Eq. 11** is simultaneously the solution of edge frequency of passband, the corresponding passband will be a straight-line coinciding with this anti-resonant frequency line. Therefore, one can determine whether a bandgap is LR bandgap by comparing the roots of **Eq. 11** with edge frequencies of the passbands. The edge frequencies can be obtained by **Eq. 9**:

$$\begin{cases} \omega^2\left(\prod_{i=1}^{n} m_i\right) f_2(\omega) = 0, \quad x = 0 \\ 4[\prod_{i=1}^{n} k_i + k(\prod_{i=1}^{n-1} m_i) f_1(\omega)] - \omega^2(\prod_{i=1}^{n} m_i) f_2(\omega) = 0, \quad x = 2. \end{cases}$$

There is a LR bandgap around a root if the root of **Eq. 11** is between the adjacent two solutions of $\omega^2 f_2(\omega) = 0$.

Based on the above inference, by comparing distributions of solutions corresponding to **Eqs 11**, **12**, we can derive an analytical parameter (p-value) or analytical discriminants describing the transition conditions between the LR bandgaps and Bragg bandgaps. The bandgap transition p-value will be defined and its analytical expression will be given in the next section (**Section 3.1**). The discriminants for a monatomic/triatomic chain will also be given in the next section (**Section 3.2**).

RESULTS AND DISCUSSION

P-value in Mass-coupled Monatomic/Diatomic Chain

Let's first discuss the simplest 2-DOF case where a monatomic chain is coupled to a diatomic chain as illustrated in **Figure 2B**. According to theories in **Section 2** and **Eq. (A3)** in **Appendix A**, the transition condition from the LR bandgap to Bragg bandgap can be written as

$$\sqrt{\frac{(M+m)(k_1+k_2)}{Mm}} < \sqrt{\frac{k_1k_2 + kk_1 + kk_2}{km}}, \tag{13}$$

i.e.,

$$p = \frac{k(k_1+k_2)(M+m)}{(k_1k_2 + kk_1 + kk_2)M} < 1, \tag{14}$$

Where p is defined as the bandgap transition parameter (p-value). If $p < 1$, there is a Bragg bandgap. Bragg bandgap turns into LR bandgap when $p > 1$.

The expression of p can be simplified as

$$p = 1 + \frac{\frac{k}{M} - \frac{k_1k_2}{(k_1+k_2)m}}{\frac{k}{m} + \frac{k_1k_2}{(k_1+k_2)m}} = 1 + \frac{\frac{k}{M} - \frac{k_{eff}}{m}}{\frac{k}{m} + \frac{k_{eff}}{m}}, \tag{15}$$

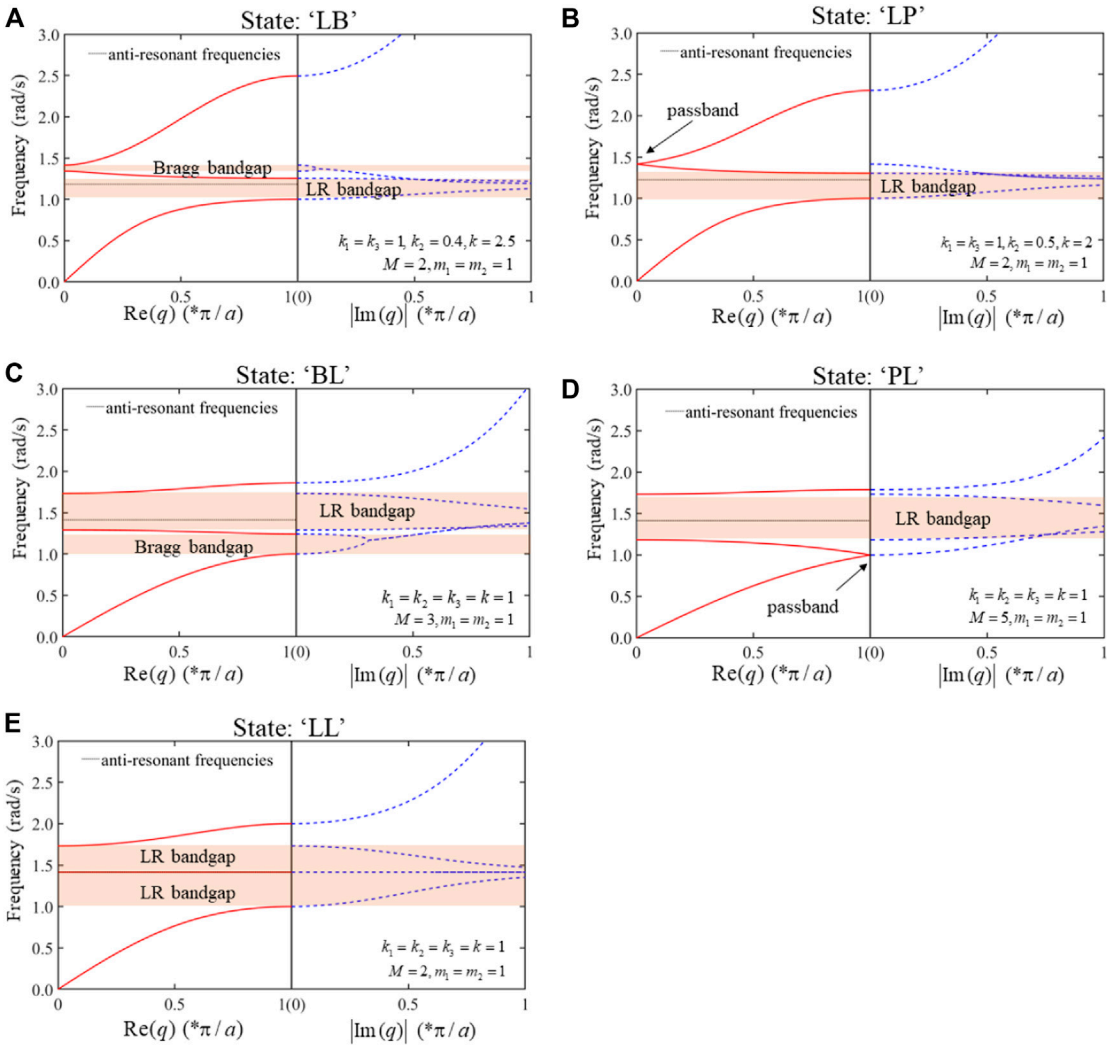

FIGURE 6 | Different bandgap states when there is only one anti-resonant frequency in the mass-coupled monatomic/triatomic chain system. **(A)** State "LB": the first bandgap is LR bandgap and second one is Bragg bandgap. **(B)** State "LP": the second Bragg bandgap disappears. **(C)** State "BL": the first bandgap is Bragg bandgap and second one is LR bandgap. **(D)** State "PL": the first Bragg bandgap has vanished and only the LR bandgap is left. **(E)** State "LL": the anti-resonant frequency line coincides with a curve of passband, which generates an enlarged LR bandgap.

Where k_{eff} is effective stiffness. It is obvious that bandgaps can be switched to different types depending on

$$\begin{cases} \frac{k}{M} > \frac{k_{eff}}{m}, & \text{Bragg bandgap to LR bandgap} \\ \frac{k}{M} < \frac{k_{eff}}{m}, & \text{LR bandgap to Bragg bandgap} \end{cases}. \tag{16}$$

In classical acoustic metamaterials with local resonators, as shown in **Figure 1B**, the value of k_{eff} is zero ($k_1 = 0$ or $k_2 = 0$), on the contrary, we get $k = 0$ in a Bragg system (*see* **Figure 1C**).

Figure 3 shows the transition process from LR bandgap to Bragg bandgap with respect to the change of p-value. If $p > 1$, the anti-resonant frequency is between the adjacent frequencies of passbands at $q = 0\,(x = 0)$, which leads to the occurrence of an anti-resonant peak in the bandgap region. Bragg bandgap appears when the anti-resonant frequency is outside the adjacent passband frequencies corresponding to$p < 1$. As shown in **Figure 3D**, Bragg bandgap will vanish in some situations due to the fact that the spring with stiffness k acts as a waveguide that counteracts and diminishes the Bragg scattering effect compared to the Bragg system.

In addition, when there is a LR bandgap, the ratio of the width of bandgap region to the maximum frequency of passbands in band structure can be calculated by

$$\eta_{LR} = \frac{\sqrt{2} - \sqrt{1 + \frac{4mk}{(M+m)(k_1+k_2)} - \sqrt{\left(1 + \frac{4mk}{(M+m)(k_1+k_2)}\right)^2 - \frac{16Mm[k_1k_2+k(k_1+k_2)]}{(M+m)^2(k_1+k_2)^2}}}}{\sqrt{\left[1 + \frac{4mk}{(M+m)(k_1+k_2)}\right] + \sqrt{\left(1 + \frac{4mk}{(M+m)(k_1+k_2)}\right)^2 - \frac{16Mm[k_1k_2+k(k_1+k_2)]}{(M+m)^2(k_1+k_2)^2}}}}. \tag{17}$$

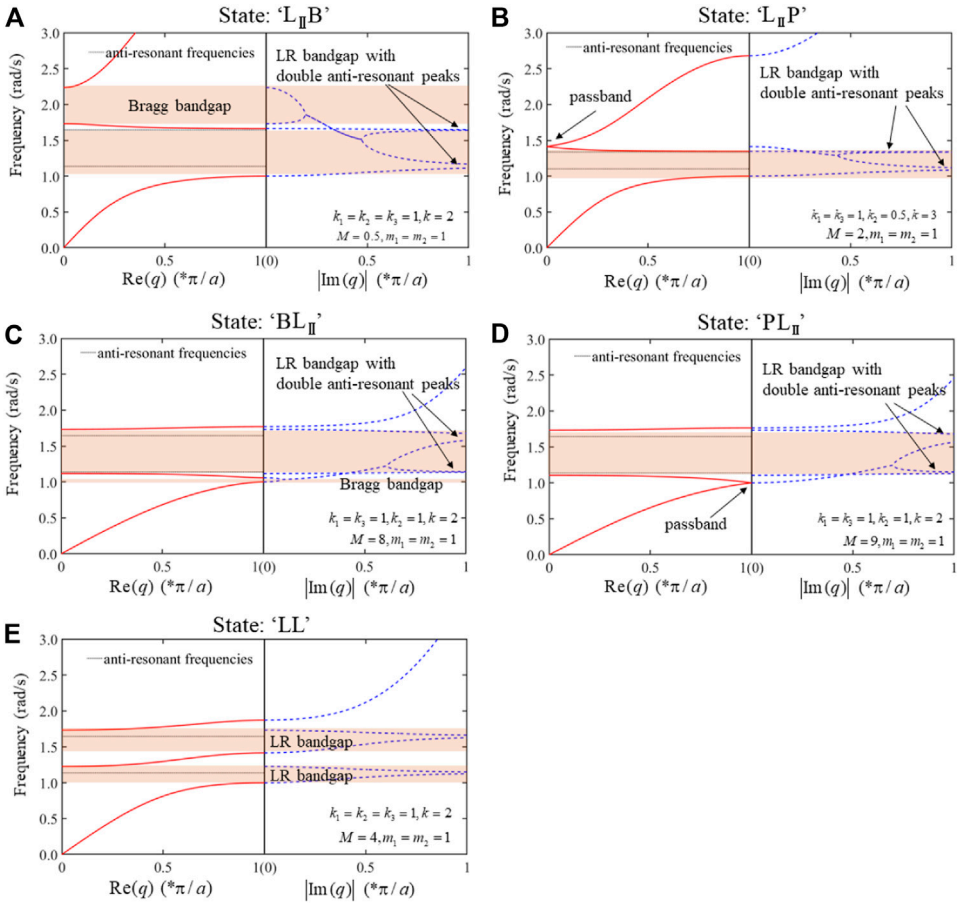

FIGURE 7 | Different bandgap states when there are two anti-resonant frequencies in the mass-coupled monatomic/triatomic chain system. **(A)** State "$L_{II}B$": the first bandgap is a LR bandgap with double anti-resonant peaks and second one is Bragg bandgap. **(B)** State "$L_{II}P$": the second Bragg bandgap becomes a passband. **(C)** State "BL_{II}": Bragg bandgap and LR bandgap with double anti-resonant peaks. **(D)** State "PL_{II}": the first Bragg bandgap vanishes. **(E)** State "LL": there are two LR bandgaps.

But for Bragg bandgap, the ratio becomes

$$\eta_{BG} = \frac{\sqrt{1+\frac{4mk}{(M+m)(k_1+k_2)}+\sqrt{\left(1+\frac{4mk}{(M+m)(k_1+k_2)}\right)^2-\frac{16Mm[k_1k_2+k(k_1+k_2)]}{(M+m)^2(k_1+k_2)^2}}}}{\sqrt{2}}$$
$$\frac{\sqrt{1+\frac{4mk}{(M+m)(k_1+k_2)}-\sqrt{\left(1+\frac{4mk}{(M+m)(k_1+k_2)}\right)^2-\frac{16Mm[k_1k_2+k(k_1+k_2)]}{(M+m)^2(k_1+k_2)^2}}}}{\sqrt{2}} \tag{18}$$

Noting that **Eq. 17** or **Eq. 18** can be expressed by three independent variables,

$$\bar{x} = \frac{k_1k_2}{(k_1+k_2)^2},\ \bar{y} = \frac{k}{(k_1+k_2)},\ \bar{z} = \frac{m}{M}, \tag{19}$$

So **Eqs 17**, **18** can be rewritten as

$$\begin{cases} \eta_{LR} = \dfrac{\sqrt{2}\sqrt{1+\bar{z}} - \sqrt{1+\bar{z}+4\bar{z}\bar{y} - \sqrt{(1+\bar{z}+4\bar{z}\bar{y})^2 - 16\bar{z}(\bar{x}+\bar{y})}}}{\sqrt{1+\bar{z}+4\bar{z}\bar{y} + \sqrt{(1+\bar{z}+4\bar{z}\bar{y})^2 - 16\bar{z}(\bar{x}+\bar{y})}}} \\ \eta_{BG} = \dfrac{\sqrt{1+\bar{z}+4\bar{z}\bar{y} + \sqrt{(1+\bar{z}+4\bar{z}\bar{y})^2 - 16\bar{z}(\bar{x}+\bar{y})}} - \sqrt{1+\bar{z}+4\bar{z}\bar{y} - \sqrt{(1+\bar{z}+4\bar{z}\bar{y})^2 - 16\bar{z}(\bar{x}+\bar{y})}}}{\sqrt{2}\sqrt{1+\bar{z}}} \end{cases}. \tag{20}$$

The discriminant of **Eq. 16** turns to

$$\begin{cases} \bar{z}\bar{y} > \bar{x}, & \text{Bragg bandgap to LR bandgap} \\ \bar{z}\bar{y} < \bar{x}, & \text{LR bandgap to Bragg bandgap} \end{cases}, \tag{21}$$

Hence the bandgap transition condition is separated by a hyperbolic paraboloid. The isosurfaces of ratios for LR bandgap and Bragg bandgap are plotted in **Figure 4** respectively. One can

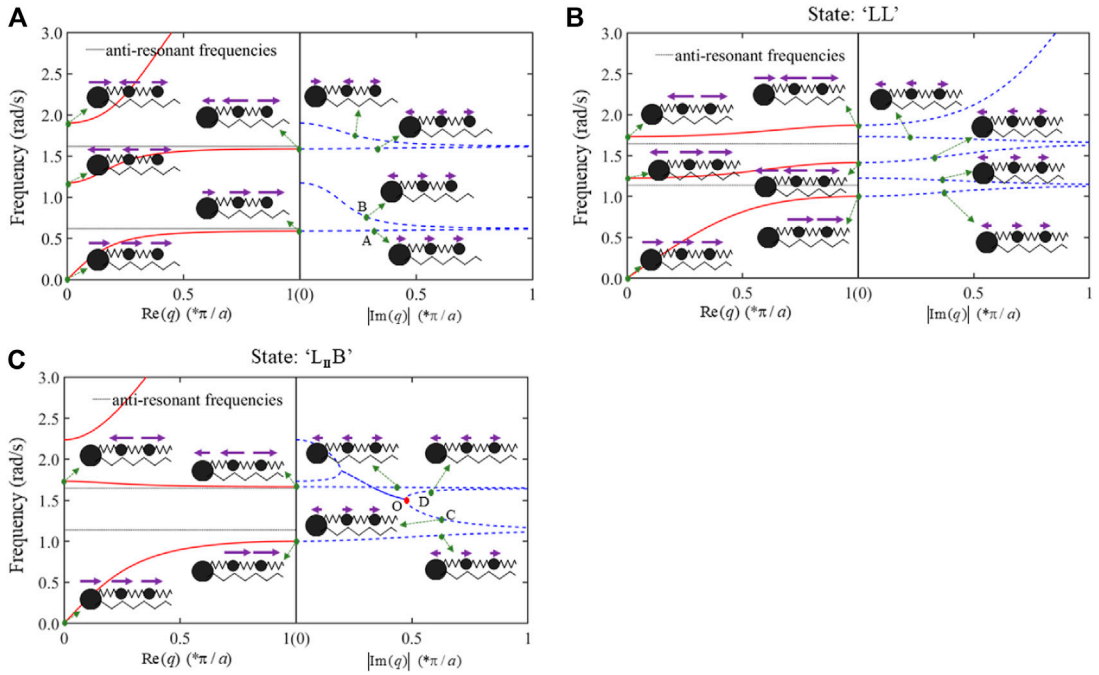

FIGURE 8 | Vibration modes of a unit cell at certain points in band structures for the **(A)** LR acoustic metamaterial with two resonators in series ($k_1 = k_2 = 1$, $k_3 = 0$, $k = 2$, $M = 0.5$, $m_1 = m_2 = 1$), **(B)** State "LL" ($k_1 = k_2 = k_3 = 1$, $k = 2$, $M = 4$, $m_1 = m_2 = 1$), and **(C)** State "$L_{II}B$" ($k_1 = k_2 = k_3 = 1$, $k = 2$, $M = 0.5$, $m_1 = m_2 = 1$). The purple arrows indicate the vibration directions and the lengths of the arrows represent the relative amplitudes. The corresponding amplitudes are zero when there are no arrows above the masses.

construct a wide bandgap at low frequency through changing the material parameters according to the isosurfaces.

Bandgap States of Mass-coupled Monatomic/triatomic Chain Classified by Discriminants

In this section, we study the 3-DOF mass-coupled monatomic/triatomic chain as shown in **Figure 2C**. Here the transition parameter p-value will turn to several sets of discriminants determining the transition conditions between LR bandgaps and Bragg bandgaps. We note that as the number of degrees of freedom further increases, the complexity of the problem sharply arises despite the number of material parameters only increase by two compared to the 2-DOF system.

According to **Eqs 9**, **11**, **12** and **Eq. (A4)**, the equations about nonzero edge frequencies of passbands can be obtained,

$$Mm_1m_2\omega^4 - ((k_1+k_3)m_1m_2 + M(k_1m_2 + k_2(m_1+m_2) + k_3m_1))\omega^2 + (k_1k_2 + k_1k_3 + k_2k_3)(m_1+m_2+M) = 0 \quad (at\ x = 0), \tag{22}$$

$$Mm_1m_2\omega^6 - [(k_1+k_3+4k)m_1m_2 + M(k_1m_2 + k_2(m_1+m_2) + k_3m_1)]\omega^4 + [(k_1k_2 + k_1k_3 + k_2k_3)(m_1+m_2+M) + 4k(k_1m_2 + k_2(m_1+m_2) + k_3m_1)]\omega^2 - 4(k_1k_2k_3 + k(k_1k_2 + k_1k_3 + k_2k_3)) = 0 \quad (at\ x = 2), \tag{23}$$

And anti-resonant frequencies can be acquired by

$$m_1m_2\omega^4 - (k_1m_2 + k_2(m_1+m_2) + k_3m_1)\omega^2 + \left(\frac{k_1k_2k_3}{k} + (k_1k_2 + k_1k_3 + k_2k_3)\right) = 0. \tag{24}$$

The distribution of solutions of these equations are discussed in detail in **Appendix B**. There are total 14 different bandgap behaviors, referred to as bandgap states, in our mass-coupled monatomic/triatomic chain according to **Eq. (B16)**. For the sake of convenience, we use "L," "B," and "P" to represent the normal LR bandgap, the Bragg bandgap, and the passband, respectively. When the values of anti-resonant frequencies solved by **Eq. 24** are conjugate imaginary numbers (i.e., anti-resonant frequencies don't actually exist), there are four different states as shown in **Figure 5**. The states from (a) to (d) correspond to sets of discriminants from (1) to (4) in **Eq. (B16)**, respectively. Obviously, there are no LR bandgaps due to non-existence of anti-resonant frequencies.

Figure 6 shows five bandgap states, corresponding to sets of discriminants from (5) to (9) in **Eq. (B16)**, where there is only one anti-resonant frequency. In **Figure 6A**, the anti-resonant frequency lies between edge frequencies of passbands, which leads to the formation of LR bandgap. The second bandgap can turn into LR bandgap with tuning of parameters as shown in **Figures 6C,D**. A widened LR bandgap is generated in **Figure 6E** due to coincidence of the anti-resonant frequency line and a dispersion curve.

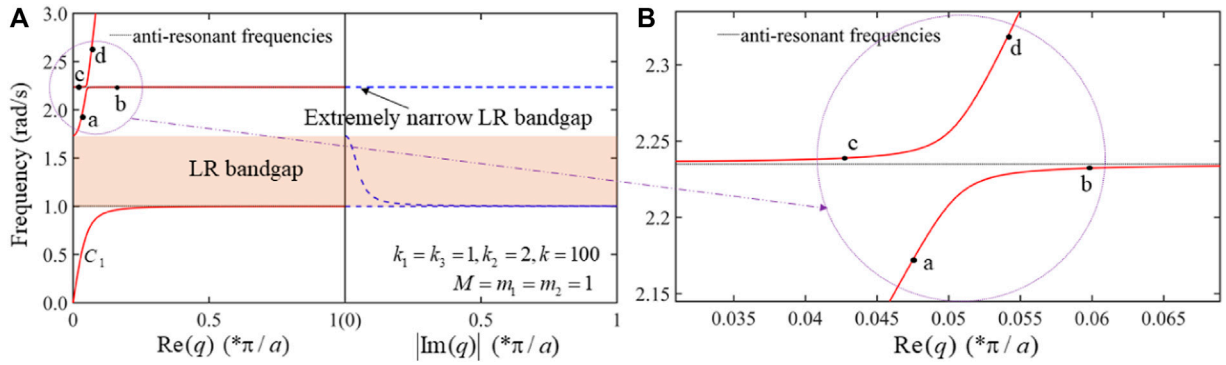

FIGURE 9 | State "LL": **(A)** the dispersion curves *ab* and *cd* veer apart in dotted circle region. **(B)** Enlarged view of the veering region.

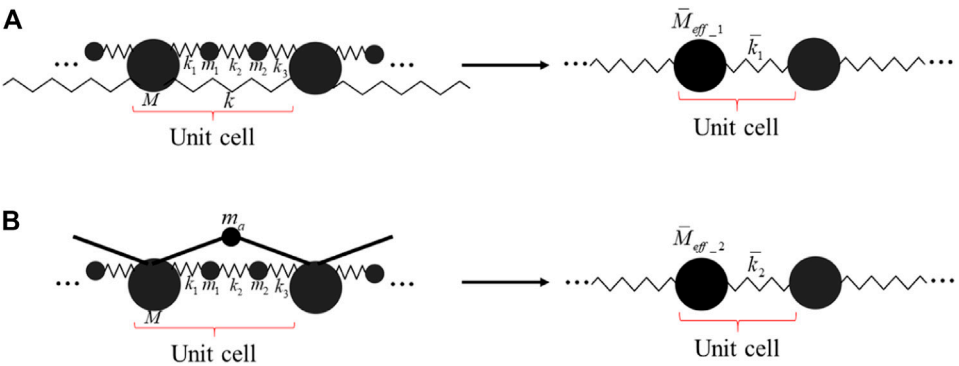

FIGURE 10 | Schematic diagrams of the effective monatomic chains for **(A)** the mass-coupled monatomic/triatomic chain (3-DOF), and **(B)** the inertial amplification system of 3-DOF.

When there are two anti-resonant frequencies, other five bandgap states arise as shown in **Figure 7**, corresponding to sets of discriminants from (10) to (14) in **Eq. (B16)**. A LR bandgap with double anti-resonant peaks is observed in **Figures 7A–D**. In order to distinguish the LR bandgap with double anti-resonant peaks from the normal LR bandgap, which is labeled as "L," the former is represented by the symbol "L_{II}." In addition, to further reveal the differences between the LR bandgap with double anti-resonant peaks and a normal one, vibration modes of a unit cell at certain points in band structures are plotted in **Figure 8**. In the LR metamaterial with two resonators in series, the anti-resonant frequencies separate two different vibration modes as shown in **Figure 8A**. Although the vibrations are attenuated and weak, all the masses vibrate in one direction at point *A* while the vibration direction of the coupled mass is different from those of the resonators at point *B*. In the state "LL" of the monatomic/triatomic chain system, the relative vibration directions of the masses are the same on both sides of the gap separated by the anti-resonant frequency as shown in **Figure 8B**. In the LR bandgap region with double anti-resonant peaks as shown in **Figure 8C**, two dispersion curves *CO* and *DO* that represent evanescent waves come close as frequency increases until the two curves lock together at point *O*, forming a pair of attenuating oscillatory waves, which later unlock into a pair of evanescent waves (Mace and Manconi, 2012). The relative vibration directions of the masses change at point *O*, so the vibration modes will ultimately change while passing through the LR bandgap region with double anti-resonant peaks.

In addition, the weak coupling phenomenon, known as veering that occurs when branches of the dispersion curves interact in coupled periodic waveguide system, is also observed in band structures in **Figure 9** (Mace and Manconi, 2012). As shown in **Figure 9**, two dispersion curves *ab* and *cd* come close together as frequency increases then the curves veer apart, which results in an extremely narrow LR bandgap.

Relations Between the Mass-coupled Monatomic/triatomic Chain and Inertial Amplification System

In the previous section, we find that under certain parameters there is a double anti-resonant peak in the LR bandgap region of the mass-coupled monatomic/triatomic chain, which is also a representative characteristic of the bandgap behaviors possessed in a periodic structure with inertial amplification mechanisms (Frandsen et al., 2016). Next, we will show that IA-like bandgaps

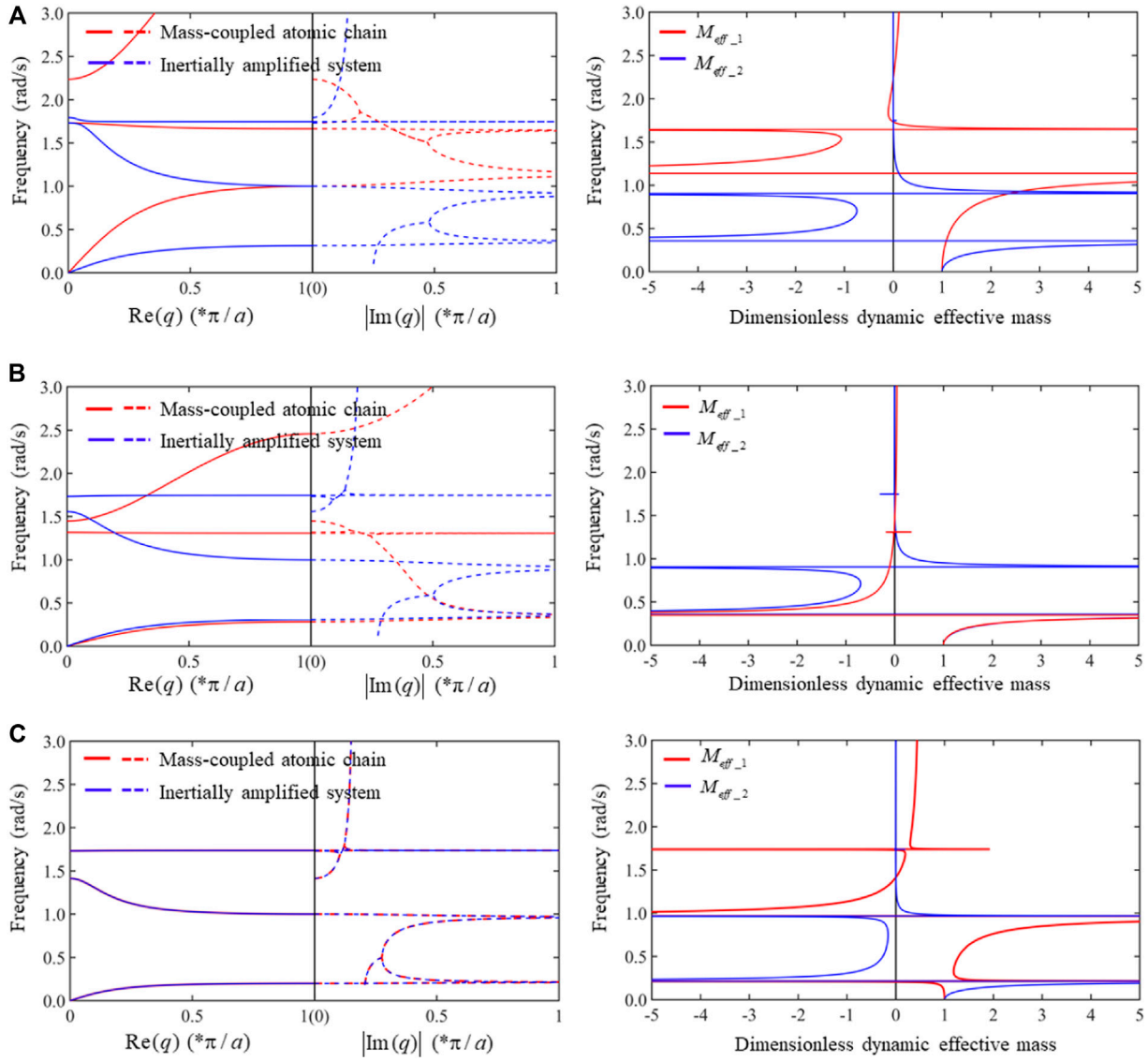

FIGURE 11 | Band structures of the mass-coupled monatomic/triatomic chains and inertial amplification systems of 3-DOF and their corresponding dimensionless dynamic effective masses. The parameters are listed as follows: **(A)** $k_1 = k_2 = k_3 = 1, k = 2, M = 0.5$, $m_1 = m_2 = 1$, $m_a = 0.4$, $\theta = \pi/18$,. **(B)** $k_1 = k_3 = k = 1, k_2 = 10, M = 1$, $m_1 = 15, m_2 = 10$for the mass-coupled atomic chain and$k_1 = k_2 = k_3 = 1, M =$ $m_1 = m_2 = 1, m_a = 0.4$, $\theta = \pi/18$for the inertial amplification system, **(C)** $k_1 = k_2 = k_3 = 1, k = \frac{1}{4}(1 - \cot^2(\pi/18))\omega^2$, $M = 2, m_1 = m_2 = 1$ for the mass-coupled atomic chain and $k_1 = k_2 = k_3 = 1, M =$ $m_1 = m_2 = 1, m_a = 1$, $\theta = \pi/18$ for the inertial amplification system.

can exist in band structures of mass-coupled monatomic/triatomic chain.

As shown in **Figure 10B**, in a classical 3-DOF inertial amplification system (Yilmaz et al., 2017), an added mass m_a is connected to the coupled masses by two massless rigid rods in a unit cell with a very small angle θ between the rigid rods and the horizontal line. The characteristic determinant of band structure is

$$\begin{vmatrix} k_1 + k_3 - \left(M + \frac{1}{2}m_a\left[1 + \cos qa + \cot^2\theta(1 - \cos qa)\right]\right)\omega^2 & -k_1 & -k_3 e^{-iqa} \\ -k_1 & k_1 + k_2 - m_1\omega^2 & -k_2 \\ -k_3 e^{iqa} & -k_2 & k_2 + k_3 - m_2\omega^2 \end{vmatrix} = 0, \tag{25}$$

Which can be rewritten as

$$\begin{aligned} &\left[M + \frac{1}{2}m_a\left(1 + \cot^2\theta\right)\right]\left[m_1 m_2\omega^6 - (k_1 m_2 + k_2(m_1 + m_2) \right. \\ &+ k_3 m_1)\omega^4 + (k_1 k_2 + k_1 k_3 + k_2 k_3)\omega^2\Big] - (k_1 + k_3)m_1 m_2\omega^4 \\ &+ (k_1 k_2 + k_1 k_3 + k_2 k_3)(m_1 + m_2)\omega^2 - 2k_1 k_2 k_3 \\ &+ \left(\frac{1}{2}m_a\left(1 - \cot^2\theta\right)\left[m_1 m_2\omega^6 - (k_1 m_2 + k_2(m_1 + m_2)\right.\right. \\ &\left.\left. + k_3 m_1)\omega^4 + (k_1 k_2 + k_1 k_3 + k_2 k_3)\omega^2\right] + 2k_1 k_2 k_3\right)\cos qa = 0. \end{aligned} \tag{26}$$

The mass-coupled atomic chain and the inertial amplification system can be simplified as effective monatomic chains. The effective stiffness and mass for the mass-coupled atomic chain are listed as

$$\begin{cases} \bar{k}_1 = \dfrac{k_1k_2k_3}{(k_1k_2+k_1k_3+k_2k_3)} + k \\ \bar{M}_{eff\_1} = \dfrac{\begin{array}{c} Mm_1m_2\omega^4 - [M(k_1m_2+k_2(m_1+m_2)+k_3m_1) \\ +(k_1+k_3)m_1m_2]\omega^2 \\ +(k_1k_2+k_1k_3+k_2k_3)(M+m_1+m_2) \end{array}}{\begin{array}{c} km_1m_2\omega^4 - k(k_1m_2+k_2(m_1+m_2)+k_3m_1)\omega^2 \\ +k(k_1k_2+k_1k_3+k_2k_3)+k_1k_2k_3 \end{array}}\bar{k}_1 \end{cases}, \tag{27}$$

And

$$\begin{cases} \bar{k}_2 = \dfrac{k_1k_2k_3}{k_1k_2+k_1k_3+k_2k_3} \\ \bar{M}_{eff\_2} = \dfrac{\begin{array}{c} (M+m_a)m_1m_2\omega^4 - [(M+m_a)(k_1m_2+k_2(m_1+m_2) \\ +k_3m_1)+(k_1+k_3)m_1m_2]\omega^2 \\ +(k_1k_2+k_1k_3+k_2k_3)(M+m_a+m_1+m_2) \end{array}}{\begin{array}{c} \frac{1}{4}m_a(1-\cot^2\theta)[m_1m_2\omega^6 - (k_1m_2+k_2(m_1+m_2) \\ +k_3m_1)\omega^4 + (k_1k_2+k_1k_3+k_2k_3)\omega^2] + k_1k_2k_3 \end{array}}\bar{k}_2 \end{cases}, \tag{28}$$

For the inertial amplification system. The dimensionless dynamic effective masses are

$$\begin{cases} M_{eff\_1} = \dfrac{\bar{M}_{eff\_1}}{M+m_1+m_2} \\ M_{eff\_2} = \dfrac{\bar{M}_{eff\_2}}{M+m_a+m_1+m_2} \end{cases}. \tag{29}$$

Besides double anti-resonant peaks, the mass-coupled atomic chain can also offer high attenuation in the bandgap regions and similar width of bandgaps compared to the inertial amplification system by adjusting material parameters (*see* **Figure 11A**). As shown in **Figures 11A,B**, a wide bandgap in low frequency can also be opened in mass-coupled atomic chain.

In fact, the band structures of the mass-coupled atomic chain can be exactly the same as that of an inertial amplification system through introducing a negative dynamic stiffness k, i.e., let

$$\begin{cases} k = \dfrac{1}{4}m_a(1-\cot^2\theta)\omega^2 \\ \bar{M} = M+m_a \end{cases}. \tag{30}$$

As seen in **Figure 11C**, the band structures are identical for these two atomic chains. The effective dynamic masses are not exactly the same because the effective stiffnesses are different when these two systems are simplified to monatomic chains according to **Eqs 27**, **28**. Thus far, we have shown that IA-like bandgaps can exist in band structures of mass-coupled monatomic/triatomic chain.

CONCLUSION

In this work, we propose an acoustic metamaterial formed by two coupled Bragg atomic chains that can possess various bandgap behaviors through the adjustment of parameters. The transition condition between LR bandgaps and Bragg bandgaps in the mass-coupled monatomic/diatomic chain can be characterized by an analytical transition parameter, referred to as p-value. If $p<1$, there is a Bragg bandgap, but the Bragg bandgap turns into LR bandgap when $p>1$. The ratio of the bandgap width to the maximum frequency of passbands is determined by three independent variables and the bandgap transition condition is separated by a hyperbolic paraboloid. A wide bandgap at low frequency can be constructed through changing the material parameters according to the isosurfaces.

The transition p-value turns to several sets of discriminants when considering bandgap states for mass-coupled monatomic/triatomic chain due to the increase of the degrees of freedom. After careful classification, we find that there are 14 different sets of discriminants, which correspond to 14 possible bandgap states. In addition, the weak coupling phenomenon termed veering which occurs in coupled periodic elastic systems is observed in the band structures. The veering phenomenon can be used to construct an extremely narrow LR bandgap. IA-like bandgaps can be opened by adjusting parameters without requirement of changing structural topological properties. Moreover, through coupling masses by a negative dynamic stiffness spring, the band structure of mass-coupled monatomic/triatomic chain system is equivalent to that of the 3-DOF inertial-amplification periodic system.

DATA AVAILABILITY STATEMENT

The raw data supporting the conclusions of this article will be made available by the authors, without undue reservation.

AUTHOR CONTRIBUTIONS

SX and K-CC conceived and designed the main ideas together; SX, ZX, and K-CC performed theoretical analysis; SX and K-CC wrote the paper draft. All authors conducted subsequent improvements to the manuscript.

FUNDING

Financial support from the National Natural Science Foundation of China (No. 11972318) and the Opening Project of State Key Laboratory for Strength and Vibration of Mechanical Structures (No. SV2020-KF-16), Xi'an Jiaotong University is gratefully acknowledged.

REFERENCES

Al Ba'ba'a, H., Nouh, M., and Singh, T. (2019). Dispersion and Topological Characteristics of Permutative Polyatomic Phononic Crystals. *Proc. R. Soc. A: Math. Phys. Eng. Sci.* 475 2226. doi:10.1098/rspa.2019.0022

Attarzadeh, M. A., Al Ba'ba'a, H., and Nouh, M. (2018). On the Wave Dispersion and Non-reciprocal Power Flow in Space-Time Traveling Acoustic Metamaterials. *Appl. Acoust.* 133, 210–214. doi:10.1016/j.apacoust.2017.12.028

Bennetts, L. G., Peter, M. A., Dylejko, P., and Skvortsov, A. (2019). Effective Properties of Acoustic Metamaterial Chains with Low-Frequency Bandgaps Controlled by the Geometry of Lightweight Mass-Link Attachments. *J. Sound Vibration* 456, 1–12. doi:10.1016/j.jsv.2019.05.022

Deymier, P. A. (2013). *Acoustic Metamaterials and Phononic Crystals*. Berlin: Springer Science and Business Media.

Fang, N., Xi, D., Xu, J., Ambati, M., Srituravanich, W., Sun, C., et al. (2006). Ultrasonic Metamaterials with Negative Modulus. *Nat. Mater* 5 (6), 452–456. doi:10.1038/nmat1644

Fang, X., Wen, J., Yin, J., and Yu, D. (2016). Wave Propagation in Nonlinear Metamaterial Multi-Atomic Chains Based on Homotopy Method. *AIP Adv.* 6 (12),121706. doi:10.1063/1.4971761

Frandsen, N. M. M., Bilal, O. R., Jensen, J. S., and Hussein, M. I. (2016). Inertial Amplification of Continuous Structures: Large Band Gaps from Small Masses. *J. Appl. Phys.* 119 (12), 124902. doi:10.1063/1.4944429

Ganesh, R., and Gonella, S. (2015). From Modal Mixing to Tunable Functional Switches in Nonlinear Phononic Crystals. *Phys. Rev. Lett.* 114 (5), 054302. doi:10.1103/PhysRevLett.114.054302

Hofmann, P. (2015). *Solid State Physics: An Introduction*. Hoboken, NJ: John Wiley & Sons.

Hu, G., Tang, L., Das, R., Gao, S., and Liu, H. (2017). Acoustic Metamaterials with Coupled Local Resonators for Broadband Vibration Suppression. *AIP Adv.* 7, 2. doi:10.1063/1.4977559

Hu, G., Tang, L., Xu, J., Lan, C., and Das, R. (2019). Metamaterial with Local Resonators Coupled by Negative Stiffness Springs for Enhanced Vibration Suppression. *J. Appl. Mech.* 86, 8. doi:10.1115/1.4043827

Huang, G. L., and Sun, C. T. (2010). Band Gaps in a Multiresonator Acoustic Metamaterial. *J. Vibration Acoust.* 132, 3. doi:10.1115/1.4000784

Huang, H. H., and Sun, C. T. (2012). Anomalous Wave Propagation in a One-Dimensional Acoustic Metamaterial Having Simultaneously Negative Mass Density and Young's Modulus. *The J. Acoust. Soc. America* 132 (4), 2887–2895. doi:10.1121/1.4744977

Huang, H. H., Sun, C. T., and Huang, G. L. (2009). On the Negative Effective Mass Density in Acoustic Metamaterials. *Int. J. Eng. Sci.* 47 (4), 610–617. doi:10.1016/j.ijengsci.2008.12.007

Jin, Y., Pennec, Y., Bonello, B., Honarvar, H., Dobrzynski, L., Djafari-Rouhani, B., et al. (2021). Physics of Surface Vibrational Resonances: Pillared Phononic Crystals, Metamaterials, and Metasurfaces. *Rep. Prog. Phys.* 84, 8. doi:10.1088/1361-6633/abdab8

Khelif, A., and Adibi, A. (2015). *Phononic Crystals*. Berlin: Springer.

Kittel, C., McEuen, P., and McEuen, P. (1996). *Introduction to Solid State Physics*. New York, NY: Wiley.

Kundu, T., Nouh, M., Aldraihem, O., and Baz, A. (2014). Metamaterial Structures with Periodic Local Resonances. San Diego, CA: Health Monitoring of Structural and Biological Systems.

Lazarov, B. S., and Jensen, J. S. (2007). Low-frequency Band Gaps in Chains with Attached Non-linear Oscillators. *Int. J. Non-Linear Mech.* 42 (10), 1186–1193. doi:10.1016/j.ijnonlinmec.2007.09.007

Li, J., and Chan, C. T. (2004). Double-negative Acoustic Metamaterial. *Phys. Rev. E Stat. Nonlin Soft Matter Phys.* 70 (5 Pt 2), 055602. doi:10.1103/PhysRevE.70.055602

Li, Y., and Zhou, W. (2021). Bandgap and Vibration Transfer Characteristics of Scissor-like Periodic Metamaterials. *J. Appl. Phys.* 130 (2). doi:10.1063/5.0047119

Liu, Y., Su, X., and Sun, C. T. (2015). Broadband Elastic Metamaterial with Single Negativity by Mimicking Lattice Systems. *J. Mech. Phys. Sol.* 74, 158–174. doi:10.1016/j.jmps.2014.09.011

Liu, Z., Zhang, X., Mao, Y., Zhu, Y. Y., Yang, Z., Chan, C. T., et al. (2000). Locally Resonant Sonic Materials. *Science* 289 (5485), 1734–1736. doi:10.1126/science.289.5485.1734

Mace, B. R., and Manconi, E. (2012). Wave Motion and Dispersion Phenomena: Veering, Locking and strong Coupling Effects. *J. Acoust. Soc. America* 131 (2), 1015–1028. doi:10.1121/1.3672647

Muhammadand Lim, C. W. (2019). Elastic Waves Propagation in Thin Plate Metamaterials and Evidence of Low Frequency Pseudo and Local Resonance Bandgaps. *Phys. Lett. A* 383 (23), 2789–2796. doi:10.1016/j.physleta.2019.05.039

Narisetti, R. K., Leamy, M. J., and Ruzzene, M. (2010). A Perturbation Approach for Predicting Wave Propagation in One-Dimensional Nonlinear Periodic Structures. *J. Vibration Acoust.* 132 (3). doi:10.1115/1.4000775

Pal, R. K., Vila, J., Leamy, M., and Ruzzene, M. (2018). Amplitude-dependent Topological Edge States in Nonlinear Phononic Lattices. *Phys. Rev. E* 97 (3-1), 032209. doi:10.1103/PhysRevE.97.032209

Porubov, A. V., and Andrianov, I. V. (2013). Nonlinear Waves in Diatomic Crystals. *Wave Motion* 50 (7), 1153–1160. doi:10.1016/j.wavemoti.2013.03.009

Pratapa, P. P., Suryanarayana, P., and Paulino, G. H. (2018). Bloch Wave Framework for Structures with Nonlocal Interactions: Application to the Design of Origami Acoustic Metamaterials. *J. Mech. Phys. Sol.* 118, 115–132. doi:10.1016/j.jmps.2018.05.012

Taniker, S., and Yilmaz, C. (2013). Phononic Gaps Induced by Inertial Amplification in BCC and FCC Lattices. *Phys. Lett. A* 377 (31-33), 1930–1936. doi:10.1016/j.physleta.2013.05.022

Vila, J., Pal, R. K., Ruzzene, M., and Trainiti, G. (2017). A Bloch-Based Procedure for Dispersion Analysis of Lattices with Periodic Time-Varying Properties. *J. Sound Vibration* 406, 363–377. doi:10.1016/j.jsv.2017.06.011

Yao, S., Zhou, X., and Hu, G. (2008). Experimental Study on Negative Effective Mass in a 1D Mass–spring System. *New J. Phys.* 10, 4. doi:10.1088/1367-2630/10/4/043020

Yilmaz, C., and Hulbert, G. M. (2017). "Dynamics of Locally Resonant and Inertially Amplified Lattice Materials," in *Dynamics of Lattice Materials*. Editors A. S. Phani and M. I. Hussein, 233–258. doi:10.1002/9781118729588.ch11

Yilmaz, C., Hulbert, G. M., and Kikuchi, N. (2007). Phononic Band Gaps Induced by Inertial Amplification in Periodic media. *Phys. Rev. B* 76, 5. doi:10.1103/physrevb.76.054309

Yilmaz, C., and Hulbert, G. M. (2010). Theory of Phononic Gaps Induced by Inertial Amplification in Finite Structures. *Phys. Lett. A* 374 (34), 3576–3584. doi:10.1016/j.physleta.2010.07.001

Yu, D., Liu, Y., Wang, G., Zhao, H., and Qiu, J. (2006). Flexural Vibration Band Gaps in Timoshenko Beams with Locally Resonant Structures. *J. Appl. Phys.* 100, 12. doi:10.1063/1.2400803

Zhu, R., Liu, X. N., Hu, G. K., Sun, C. T., and Huang, G. L. (2014). A Chiral Elastic Metamaterial Beam for Broadband Vibration Suppression. *J. Sound Vibration* 333 (10), 2759–2773. doi:10.1016/j.jsv.2014.01.009

Zucker, I. J. (2016). 92.34 The Cubic Equation - A New Look at the Irreducible Case. *Math. Gaz.* 92 (524), 264–268. doi:10.1017/s0025557200183135

Conflict of Interest: The authors declare that the research was conducted in the absence of any commercial or financial relationships that could be construed as a potential conflict of interest.

Publisher's Note: All claims expressed in this article are solely those of the authors and do not necessarily represent those of their affiliated organizations, or those of the publisher, the editors and the reviewers. Any product that may be evaluated in this article, or claim that may be made by its manufacturer, is not guaranteed or endorsed by the publisher.

APPENDIX A

(Note: All material parameters discussed in Appendix A and B are positive by default.)

The analytical formulas of $f_1(\omega)$ and $f_2(\omega)$ in **Eq. 9** are expressed as

$$\begin{cases} f_1(\omega) = \sum_{i=1}^{n}(-1)^{i-1}\left(\sum_{z_1<z_2<\cdots<z_{n-i}}^{z_1,z_2,\cdots z_{n-i}\in[1,n-1]} \frac{\sum_{t_1<t_2<\cdots<t_{n-i}}^{k_{t_s}\in\{k_{z_s},k_{z_s+1}\}}\left(\prod_{s=1}^{n-i}k_{t_s}\right)}{\prod_{s=1}^{n-i}m_{z_s}}\right)\omega^{2(i-1)} \\ f_2(\omega) = \sum_{i=1}^{n}(-1)^{i-1}\left(\sum_{z_1<z_2<\cdots<z_{n-i}}^{z_1,z_2,\cdots z_{n-i}\in[1,n]} \frac{\sum_{t_1<t_2<\cdots<t_{n-i}}^{k_{t_s}\in\{k_{z_s},k_{z_s+1}\}}\left(\prod_{s=1}^{n-i}k_{t_s}\right)}{\prod_{s=1}^{n-i}m_{z_s}}\right)\omega^{2(i-1)} \end{cases}, \tag{A1}$$

where

$$m_n = M,\ k_{n+1} = k_1, \tag{A2}$$

noting that value range of z_s is $[1, n-1]$ in $f_1(\omega)$ but that of z_s is $[1, n]$ in $f_2(\omega)$. This is because there is one more component (i.e., coupled mass M) in $f_2(\omega)$.

Some concrete expressions are as follows:

$$\begin{cases} f_1(\omega) = -\omega^2 + \frac{k_1+k_2}{m_1} \\ f_2(\omega) = -\omega^2 + \frac{(M+m_1)}{Mm_1}(k_1+k_2) \end{cases} \quad \text{for n = 2,} \tag{A3}$$

When $n = 3$,

$$\begin{cases} f_1(\omega) = \omega^4 - \frac{(k_1m_2+k_2(m_1+m_2)+k_3m_1)}{m_1m_2}\omega^2 + \frac{(k_1k_2+k_1k_3+k_2k_3)}{m_1m_2} \\ f_2(\omega) = \omega^4 - \left(\frac{k_1+k_3}{M} + \frac{(k_1m_2+k_2(m_1+m_2)+k_3m_1)}{m_1m_2}\right)\omega^2 \\ \qquad + (k_1k_2+k_1k_3+k_2k_3)\frac{(m_1+m_2+M)}{Mm_1m_2} \end{cases}, \tag{A4}$$

when $n = 4$,

$$\begin{aligned} f_1(\omega) = -\omega^6 &+ \left(\frac{k_1m_2m_3 + k_2(m_1+m_2)m_3}{m_1m_2m_3} + \frac{+k_3(m_2+m_3)m_1 + k_4m_1m_2}{m_1m_2m_3}\right)\omega^4 \\ &- \left(\frac{m_1(k_2k_3+k_2k_4+k_3k_4)}{m_1m_2m_3} + \frac{+m_2(k_1k_3+k_1k_4+k_2k_3+k_2k_4)}{m_1m_2m_3} + \frac{+m_3(k_1k_2+k_1k_3+k_2k_3)}{m_1m_2m_3}\right)\omega^2 \\ &+ \frac{k_1k_2k_3+k_1k_2k_4+k_1k_3k_4+k_2k_3k_4}{m_1m_2m_3}, \end{aligned} \tag{A5}$$

$$\begin{aligned} f_2(\omega) = -\omega^6 &+ \left(\frac{(k_1+k_4)}{M} + \frac{k_1m_2m_3 + k_2(m_1+m_2)m_3}{m_1m_2m_3} + \frac{+k_3(m_2+m_3)m_1 + k_4m_1m_2}{m_1m_2m_3}\right)\omega^4 \\ &- \left(\frac{m_1(k_2k_3+k_2k_4+k_3k_4) + m_2(k_1k_3}{m_1m_2m_3} + \frac{+k_1k_4+k_2k_3+k_2k_4) + m_3(k_1k_2+k_1k_3+k_2k_3)}{m_1m_2m_3} \right. \\ &\left. + \frac{(k_1k_3+k_1k_4+k_3k_4)}{Mm_3}\right)\omega^2 \\ &+ \frac{(k_1k_2+k_2k_4+k_1k_3+k_3k_4)}{Mm_2} + \frac{(k_1k_2+k_1k_4+k_2k_4)}{Mm_1} \\ &+ (k_1k_2k_3+k_1k_2k_4+k_1k_3k_4+k_2k_3k_4)\frac{(m_1+m_2+m_3+M)}{Mm_1m_2m_3}. \end{aligned} \tag{A6}$$

APPENDIX B

We will solve **Eq. 22** as well as **Eq. 24** and make a thorough classified discussion to obtain the discriminants about bandgap transitions.

The criterion on existence of solutions of **Eq. 22** is:

$$\begin{aligned} \Delta_1 = &\left((k_1+k_3)m_1m_2 + M(k_1m_2 + k_2(m_1+m_2) + k_3m_1)\right)^2 \\ &- 4Mm_1m_2(k_1k_2+k_1k_3+k_2k_3)(m_1+m_2+M), \end{aligned} \tag{B1}$$

and for **Eq. 24** it becomes

$$\begin{aligned} \Delta_2 = &(k_1m_2 + k_2(m_1+m_2) + k_3m_1)^2 - 4m_1m_2\left(\frac{k_1k_2k_3}{k} + (k_1k_2\right. \\ &\left. + k_1k_3 + k_2k_3)\right). \end{aligned} \tag{B2}$$

First, we will confirm that **Eq. (B1)** is always greater than or equal to zero, i.e.,

$$\Delta_1 \geq 0. \tag{B3}$$

The **Eq. (B1)** can be written as function of M:

$$\begin{aligned} f(M) = &M^2\left(\left(-k_1m_2 + k_2m_1 - k_2m_2 + k_3m_1\right)^2 + 4k_2^2m_1m_2\right) \\ &+ 2M\left(k_1^2m_1m_2^2 + k_3^2m_1^2m_2 - (k_1k_2 + k_1k_3\right. \\ &\left.+k_2k_3)\left(m_1^2m_2 + m_1m_2^2\right)\right) \\ &+ (k_1+k_3)^2m_1^2m_2^2, \end{aligned} \tag{B4}$$

then the criterion on roots of this quadratic function is

$$\bar{\Delta}_1 = -4(k_1k_2+k_1k_3+k_2k_3)(k_1m_2 - k_3m_1)^2 \leq 0. \tag{B5}$$

Therefore, **Eq. (B3)** has been proven to be correct for all situations.

Next, we will discuss the following six situations:

$$\begin{cases} \Delta_1 > 0 \\ \Delta_2 < 0 \end{cases}, \begin{cases} \Delta_1 = 0 \\ \Delta_2 < 0 \end{cases}, \begin{cases} \Delta_1 > 0 \\ \Delta_2 = 0 \end{cases}, \begin{cases} \Delta_1 = 0 \\ \Delta_2 = 0 \end{cases}, \begin{cases} \Delta_1 > 0 \\ \Delta_2 > 0 \end{cases}, \text{ and } \begin{cases} \Delta_1 = 0 \\ \Delta_2 > 0 \end{cases}. \tag{B6}$$

The equivalent formulas below can be derived:

$$\Delta_1 = 0 \Leftrightarrow (k_1 m_2 - k_3 m_1)^2 + \left[(k_1 + k_3)\frac{m_1 m_2}{M} - k_2 (m_1 + m_2) \right]^2 = 0 \tag{B7}$$

and

$$\Delta_2 = 0 \Leftrightarrow (- k_1 m_2 + k_2 m_1 - k_2 m_2 + k_3 m_1)^2 + 4k_2^2 m_1 m_2 - 4m_1 m_2 \frac{k_1 k_2 k_3}{k} = 0. \tag{B8}$$

Solutions of **Eq. 22** can be expressed as

$$\bar{\omega}_{1,2} = \sqrt{\frac{(k_1 + k_3) m_1 m_2 + M (k_1 m_2 + k_2 (m_1 + m_2) + k_3 m_1) \pm \sqrt{\Delta_1}}{2M m_1 m_2}}, \tag{B9}$$

and those of **Eq. 24** are

$$\bar{\omega}_{LR_1, LR_2} = \sqrt{\frac{k_1 m_2 + k_2 (m_1 + m_2) + k_3 m_1 \pm \sqrt{\Delta_2}}{2 m_1 m_2}}. \tag{B10}$$

For every situation in Eq. (B6), the classified discussions are carried forward by comparing the distribution between solutions of **Eq. 22** and that of **Eq. 24**. Several sets of discriminants, which are used to distinguish different bandgap behaviors, of all possible results of discussions are listed below,

$$\begin{cases} g_1 > 0 \\ g_2 < 0 \end{cases}, \quad \begin{cases} g_1 = 0 \\ g_2 < 0 \end{cases}, \quad \begin{cases} g_1 > 0 \\ g_2 = 0, \\ g_3 < 0 \end{cases} \quad \begin{cases} g_1 > 0 \\ g_2 = 0, \\ g_3 = 0 \end{cases} \quad \begin{cases} g_1 > 0 \\ g_2 = 0, \\ g_3 > 0 \end{cases}$$
$$\begin{cases} g_1 = 0 \\ g_2 = 0 \end{cases}, \quad \begin{cases} g_1 = 0 \\ g_2 > 0 \end{cases}, \quad \begin{cases} g_1 > 0 \\ g_2 > 0, \\ g_3 \le 0 \end{cases} \quad \begin{cases} g_1 > 0 \\ g_2 > 0 \\ g_3 \ge 0, \\ g_4 > 0 \end{cases} \quad \begin{cases} g_1 > 0 \\ g_2 > 0 \\ g_3 < 0, \\ g_4 > 0 \end{cases} \tag{B11}$$

where $g_i\,(i = 1, 2, 3, 4)$ are functions of material parameters:

$$\begin{cases} g_1 (M, k_1, k_2, k_3, m_1, m_2) = (k_1 m_2 - k_3 m_1)^2 + \left[(k_1 + k_3)\frac{m_1 m_2}{M} - k_2 (m_1 + m_2) \right]^2 \\ g_2 (k, k_1, k_2, k_3, m_1, m_2) = (- k_1 m_2 + k_2 m_1 - k_2 m_2 + k_3 m_1)^2 + 4k_2^2 m_1 m_2 - 4m_1 m_2 \frac{k_1 k_2 k_3}{k} \\ g_3 (M, k_1, k_2, k_3, m_1, m_2) \\ \quad = M\left((- k_1 m_2 + k_2 m_1 - k_2 m_2 + k_3 m_1)^2 + 4k_2^2 m_1 m_2 \right) \\ \quad - 2m_1 m_2 \left[(k_1 k_2 + k_1 k_3 + k_2 k_3)(m_1 + m_2) \right. \\ \quad \left. - (k_1^2 m_2 + k_3^2 m_1) \right] g_4 (k, M, k_1, k_2, k_3, m_1, m_2) \\ \quad = \left(\frac{k_1 k_2 k_3}{k} \right)^2 M^2 - \frac{k_1 k_2 k_3}{k} M \left[(k_1 k_2 + k_1 k_3 + k_2 k_3)(m_1 + m_2) \right. \\ \quad \left. - (k_1^2 m_2 + k_3^2 m_1) \right] \\ + (k_1 + k_3)^2 \frac{k_1 k_2 k_3}{k} m_1 m_2 - (k_1 k_2 + k_1 k_3 + k_2 k_3)(k_1 m_2 - k_3 m_1)^2. \end{cases} \tag{B12}$$

The above results have not included the influence of frequencies of passbands at another edge (i.e., $q = \pi/a, x = 2$). In fact, the distribution of frequencies at $x = 2$ only affects whether the Bragg bandgaps are opened or not after we have determined locations of LR bandgaps. Then we will deal with equation about edge ($x = 2$) frequencies of passbands (i.e., **Eq. 23**). According to theories about solutions of cubic equation (Zucker, 2016), its discriminants of the roots are:

$$\begin{cases} \Delta_{r1} = 18\bar{a}\bar{b}\bar{c}\bar{d} - 4\bar{b}^3\bar{d} + \bar{b}^2\bar{c}^2 - 4\bar{a}\bar{c}^3 - 27\bar{a}^2\bar{d}^2 \\ \Delta_{r2} = \bar{b}^2 - 3\bar{a}\bar{c} \end{cases}, \tag{B13}$$

where

$$\begin{cases} \bar{a} = M m_1 m_2 \\ \bar{b} = -[(k_1 + k_3 + 4k) m_1 m_2 + M (k_1 m_2 + k_2 (m_1 + m_2) + k_3 m_1)] \\ \bar{c} = (k_1 k_2 + k_1 k_3 + k_2 k_3)(m_1 + m_2 + M) \\ \quad + 4k (k_1 m_2 + k_2 (m_1 + m_2) + k_3 m_1) \\ \bar{d} = -4 (k_1 k_2 k_3 + k (k_1 k_2 + k_1 k_3 + k_2 k_3)). \end{cases} \tag{B14}$$

Adopting similar approaches on proving Eq. (B3), one can ascertain the following inequalities

$$\begin{cases} \Delta_{r1} \ge 0 \\ \Delta_{r2} > 0 \end{cases} \tag{B15}$$

are true for any material parameters. It means that Eq. (B13) has three distinct real roots or has a double real root as well as a single real root. The Bragg bandgaps at $x = 2\,(q = \pi/a)$ will be opened when $\Delta_{r1} > 0$ and will be closed when $\Delta_{r1} = 0$.

The final sets of discriminants are as follows after above discussion:

$$\begin{gathered} (1)\begin{cases} g_1 > 0 \\ g_2 < 0 \\ \Delta_{r1} > 0 \end{cases}, (2)\begin{cases} g_1 > 0 \\ g_2 < 0 \\ \Delta_{r1} = 0 \end{cases}, (3)\begin{cases} g_1 = 0 \\ g_2 < 0 \\ \Delta_{r1} > 0 \end{cases}, \\ (4)\begin{cases} g_1 = 0 \\ g_2 < 0 \\ \Delta_{r1} = 0 \end{cases}, (5)\begin{cases} g_1 > 0 \\ g_2 = 0, \\ g_3 < 0 \end{cases} (6)\begin{cases} g_1 = 0 \\ g_2 = 0 \end{cases}, \\ (7)\begin{cases} g_1 > 0 \\ g_2 = 0 \\ g_3 > 0 \\ \Delta_{r1} > 0 \end{cases}, (8)\begin{cases} g_1 > 0 \\ g_2 = 0 \\ g_3 > 0 \\ \Delta_{r1} = 0 \end{cases}, (9)\begin{cases} g_1 > 0 \\ g_2 = 0, \\ g_3 = 0 \end{cases} \\ (10)\begin{cases} g_1 > 0 \\ g_2 > 0 \\ g_3 < 0 \\ g_4 > 0 \end{cases}, (11)\begin{cases} g_1 = 0 \\ g_2 > 0 \end{cases}, \\ (12)\begin{cases} g_1 > 0 \\ g_2 > 0 \\ g_3 \ge 0 \\ g_4 > 0 \\ \Delta_{r1} > 0 \end{cases}, (13)\begin{cases} g_1 > 0 \\ g_2 > 0 \\ g_3 \ge 0 \\ g_4 > 0 \\ \Delta_{r1} = 0 \end{cases}, (14)\begin{cases} g_1 > 0 \\ g_2 > 0, \\ g_4 \le 0 \end{cases} \end{gathered} \tag{B16}$$

where each set of discriminants corresponds to a bandgap behavior in the mass-coupled monatomic/triatomic chain system.